Infrared Physics & Technology 140 (2024) 105394

Contents lists available at ScienceDirect

Infrared Physics and Technology

journal homepage: www.elsevier.com/locate/infrared

Research Paper

Conduction thermography for non-destructive assessment of fatigue cracks in metallic materials

Ester D'Accardi [a,*], Rosa De Finis [b], Giuseppe Dell'Avvocato [c], Giuseppe Masciopinto [a], Davide Palumbo [a], Umberto Galietti [a]

[a] Department of Mechanics, Mathematics and Management (DMMM), Polytechnic University of Bari, Via Edoardo Orabona n. 4, 70125 Bari, BA, Italy
[b] Innovation Engineering Department, University of Salento, Campus Ecotekne build. O-S.P. 6, Via Lecce Monteroni, 73100 LECCE, LE, Italy
[c] University of L'Aquila, Industrial and Information Engineering and Economics, Piazzale Ernesto Pontieri 1, Monteluco di Roio, 67100 L'Aquila, AQ, Italy

ARTICLE INFO

Keywords:
Conduction Thermography (CT)
Thermoelastic Stress Analysis (TSA)
Fatigue cracks
Current
Titanium

ABSTRACT

Metallic materials are widely used in many applications of mechanical and aerospace engineering. Due to severe environmental and loading conditions, components and structures can experience cracking phenomena. In this regard, different non-destructive techniques were developed in the last years to detect and monitor cracks that can propagate during the actual loading conditions.

This work deals with the application of the conduction thermography as a non-destructive technique for the offline control and inspection of different notched metallic specimens characterized by short fatigue cracks. The potentials of the technique have been demonstrated considering a low-cost set-up consisting of a power supply of low current and limited voltage, and a microbolometer sensor. Moreover, to further simplify the inspection, the specimens were not black coated. Quantitative results, in terms of crack lengths, have been obtained using a new procedure of data analysis and then compared to those provided by thermoelastic stress analysis, a well-established technique adopted for the detection and monitoring of cracks.

1. Introduction

Fatigue and corrosion can significantly reduce the life of metallic components, due to the onset of cracks that can lead to unexpected in-service failures. So, timely detecting and characterising short fatigue cracks is vital to increase safety and reliability in engineering fields such as aeronautical, aerospace and mechanical one [1–4].

According to Standards [5], there are well-established non-destructive techniques (NDT) that can be used for detecting cracks including penetrants testing, magnetic particle inspection, and X-ray techniques. These methods are time consuming, require the contact with the inspected component and do not provide the possibility of automation in industrial field [3,6–8]. Furthermore, the non-destructive inspection with traditional techniques is usually applied offline, when inspected components are not operating. Furthermore, some traditional NDT can fail in detecting short cracks in absence of external loads, leading to the crack closure phenomenon. This latter issue is critical especially during standard ultrasonic testing [7,8].

To overcome these problems, active thermography (AT) techniques such as induction (IT), conduction thermography (CT), thermoelastic stress analysis (TSA), and flying laser thermography (FLT) can be applied [12–16].

Approaches based on IT or CT involve the injection of certain level current (normally >200 A) in the inspected component. The current density distribution increases around the crack tips, causing the apparent temperature to significantly increase with respect to the sound areas [17–22].

As demonstrated in the last years [12–14,21,22], if IT can be considered well-established for crack detection and characterization in many applications, the use of conduction thermography is instead less widespread, probably due to lack of research works that deeply investigated the experimental set-up and possible in-situ applications [12,17–20]. There are, in fact, very few and old publications that proposed and discussed the use of CT considering the typical constrains related to in-service inspections such as, the need for contact with the component and safety problems due to the use of high electrical currents

* Corresponding author.
E-mail addresses: ester.daccardi@poliba.it (E. D'Accardi), rosa.definis@unisalento.it (R. De Finis), giuseppe.dellavvocato@univaq.it (G. Dell'Avvocato), g.masciopinto@phd.poliba.it (G. Masciopinto), davide.palumbo@poliba.it (D. Palumbo), umberto.galietti@poliba.it (U. Galietti).

https://doi.org/10.1016/j.infrared.2024.105394
Received 26 February 2024; Received in revised form 28 May 2024; Accepted 5 June 2024
Available online 10 June 2024

and high voltage [12,17,18]. Moreover, the large part of literature works focused on the use of an alternate current (AC) rather than the direct current (DC), and then on detecting superficial cracks. Instead, the use of DCs has less explored even if this approach allowing the inspection of deeper depths with respect to AC and then detecting sub-surface cracks [19,20,23].

Furthermore, CT has peculiar advantages with respect to well-established AT techniques.

As an example, IT can present some issues related to the use of coil-specific geometries that, in turn, influences the crack detection and limits the inspection to defined portions of the component. Furthermore, the edge effects can influence crack detection, reducing the probability of detection and the reliability of IT.

FLT, often used for crack detection [24–28], requires a scan of the component, which extends testing and post processing times, while TSA can be only performed in presence of external dynamic loads applied to the component [9–11]. Moreover, due to the nature of the thermoelastic effect, a matt black need to be used to increase the surface emissivity and enhance the signal to noise ratio.

This work aims to investigate and quantitatively assess the feasibility of CT to detect and measure short cracks. A low-cost setup is proposed and used based on preliminary results shown in the short abstract [23]. An experimental campaign was conducted to inspect several thin specimens of different materials, mainly adopting a microbolometer sensor and a switching power supply in DC.

Moreover, a novel procedure for crack detection and crack length estimation is also proposed, based on processing thermal data over time and using the determination coefficient (R^2) as an index to describe the thermal behaviour of the crack during the transient heating phase.

To demonstrate the potential of the technique, several experimental tests were carried out considering different notch geometries, on different materials such as a titanium alloy, and two steels, austenitic and ferromagnetic one.

The goal was to demonstrate the feasibility of the technique by expanding the application range from ferrous metal to non-ferrous ones, from high-diffusive to lower ones, covering a large range of different electrical properties. Moreover, the influence of some testing parameters, i.e. the current level or time of excitation has been investigated on the titanium alloy Ti6Al4V, commonly used to manufacture aerospace components such as, turbine blades that make up key components, including gas turbine axial compressors and rotors [3,4]. It was demonstrated that titanium is a good candidate to be inspected with conduction thermography thanks to its material properties characterized by low values of both electrical conductivity and thermal diffusivity that allow to reduce the level of current used for the tests.

The quantitative results were compared with those obtained by applying TSA, that is considered in this work the reference method for crack tip identification and crack length estimation.

2. Material and methods

This section reports materials and methods, starting from preliminary considerations achieved by simulating the phenomenon with an FE model to understand the expected temperature increase in the proximity of the crack tip. The experimental setups adopted for cyclic tests to generate short fatigue cracks and for non-destructive evaluation with CT will be presented. The specific algorithm proposed to analyse the raw thermal data from conduction tests and the procedure adopted to obtain crack length measurement are here described in detail.

2.1. Numerical model

To investigate the thermal and electrical behaviour of thin specimens of different materials, a numerical model has been developed in COMSOL Multiphysics®. The aim is to simulate the electrical and thermal behaviour when a potential difference is applied at opposite sides of the specimen.

In the FE model, the discretization was performed using second-order tetrahedral elements, with a finer mesh adopted in regions experiencing higher thermal gradients. The developed model is a multi-physics model as it encompasses both thermal aspects, where the heat source arises from Joule heating due to current passing through the specimen. For the generation of heat due to current, it is necessary to consider the following three equations:

$$\nabla \bullet \boldsymbol{J} = Q \tag{1}$$

This equation states the divergence of the current density $\boldsymbol{J}$, within a volume equals the charge generation rate per unit volume, Q. In this case, it expresses the conservation of the charge.

$$\boldsymbol{J} = \sigma \boldsymbol{E} + \frac{\partial \boldsymbol{D}}{\partial t} + \boldsymbol{J}_e \tag{2}$$

Eq. (2) represents the constitutive relation for current density and defines the total current density as a sum of conduction current ($\sigma \boldsymbol{E}$), displacement current ($\frac{\partial \boldsymbol{D}}{\partial t}$), and an external current density ($\boldsymbol{J}_e$), where σ is the electrical conductivity and $\boldsymbol{E}$ the electrical field intensity which is described in (3), as the negative gradient of the electrical potential V.

$$\boldsymbol{E} = -\nabla V \tag{3}$$

For the thermal aspect of the problem, we can express the conservation of heat and Fourier's law of heat conduction:

$$\rho c_p \frac{\partial T}{\partial t} + \rho c_p \boldsymbol{U} \bullet \nabla T + \nabla \bullet \boldsymbol{q} = Q \tag{4}$$

It accounts for heat accumulation ($\rho c_p \frac{\partial T}{\partial t}$), the transportation term ($\rho c_p \boldsymbol{U} \bullet \nabla T$) and conductive heat transfer ($\nabla \bullet \boldsymbol{q}$), equating them to the rate of heat generation, Q. ρ is the density, c_p is the specific heat at constant pressure, T is the temperature, $\boldsymbol{U}$ the velocity field and $\boldsymbol{q}$ the heat flux which is proportional to the negative gradient of the temperature, indicating that heat flows from regions of high temperature to regions of low temperature. k is the thermal conductivity.

$$\boldsymbol{q} = -k \nabla T \tag{5}$$

A transient problem was solved with a time step of 0.1 ms, ranging from 0 to about 1800 ms.

$$\rho c_p \frac{\partial T}{\partial t} + \rho c_p \boldsymbol{U} \bullet \nabla T + \nabla \bullet (-k \nabla T) = \frac{1}{\sigma} |\boldsymbol{J}|^2 \tag{6}$$

To have an idea of the effective potential of the technique in the presence of a crack, the simulation included in the geometry a crack of about 2 mm, and the presence of a notch in the centre of the specimen.

In the considered simulation, a crack length of 2 mm was hypothesized on a 3 mm specimen. Based on the properties of titanium and considering the crack faces as two flat surfaces in contact at a distance of 1 μm, the resistance was estimated. Consequently, the conductance was found to be 1.43×10^7 S. These values yielded results consistent with the experimental ones, as shown after in the results. This value is indicative and derived from an estimate without considering the influences of other factors.

2.2. Experimental campaign, specimens and equipment

Three metallic materials (one specimen per material) have been tested (Fig. 1), offline, without loading on machine: a titanium alloy (Ti-6Al-4V – specimen 1, S1), a ferromagnetic steel (specimens 2, S2), and an austenitic one (AISI 304 – specimen 3, S3). After the preliminary results obtained in [23], to increase the case history, other notched geometries have been investigated analysing two steel specimens (indicated as S4 and S5) as reported in Table 1 and Fig. 1. Moreover, as

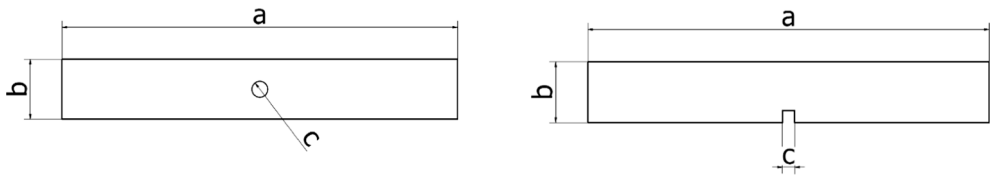

Fig. 1. A schematic representation of specimen geometry (a) hole in the centre, (b) notch of square shape.

Table 1
Material and geometrical characteristics of the investigated specimens.

Specimen (ID)	Material	a (mm)	b (mm)	Thickness (mm)	Notch dimension – c (mm)
S1	titanium alloy Ti-6Al-4V	200	40	3	4
S2	austenitic steel	200	30	1	
S4	AISI 304				
S3	ferromagnetic	200	30	1	
S5	steel Fe360				

Table 2
Camera parameters and Loading conditions for TSA tests.

Camera parameters and Loading conditions for TSA tests					
Loading machine Model MTS 370 Load frame, ±100kN	Specimen (ID)	Load frequency [Hz]	R	$\sigma_{max,\ nom}$ [MPa]	Cycles number
	S1	10	0.5	83	25,000
	S2 and S3	13	0.1	320	14,000
	S4 and S5	13	0.1	320	36,000
Cooled camera FLIR X6540sc, MWIR 3–5 μm, NETD < 25 mk, 640x512 pixels Frame rate 200 Hz Geometrical resolution 0.15 mm/pixel Acquisition duration 10 s					

suggested by the preliminary results of FE simulations, the effect of the cross section has been investigated as it can significantly influence the crack detectability for given values of current and heating time.

Small fatigue cracks have been generated around notched regions performing cyclic tests with increasing loads (until crack arises), by means of with a servo-hydraulic fatigue machine (MTS 370, 100 kN capacity), Fig. 2. As a reference, the thermoelastic data have been collected using an infrared-cooled camera FLIR X6540sc with an indium-antimonium detector. The acquisition parameters and loading table are reported in Table 2. For TSA tests, as known [9,11], all the specimens must be covered with matt black coating to increase the surface emissivity up to about 0.95.

Non-destructive conduction tests have been carried out with the set-up shown in Fig. 3, considering two different infrared cameras placed on the opposite sides of the specimen in order to evaluate the crack length on both surfaces. In particular, the same cooled camera FLIR X6540sc has been used on one side and a microbolometer FLIR A655sc (a cheaper sensor) on the opposite side. The geometrical resolution was almost the same.

The current excitation has been applied at the opposite edges of the specimen with two cables and two clamps (interposing a thick copper sheet between the specimen surface and clamp itself) controlling a switching power supply (83.3 A, 12 V), coupled with electrical resistors placed in series with the test specimens to avoid short circuits. To fix the pulse duration, a function generator and a solid state relay have been adopted to open and close the circuit. A clamp ammeter has been used to check the effective current value for each test.

Different tests have been performed according to Table 3 by changing the test parameters, repeating the tests 3 times and considering the specimens coated and not.

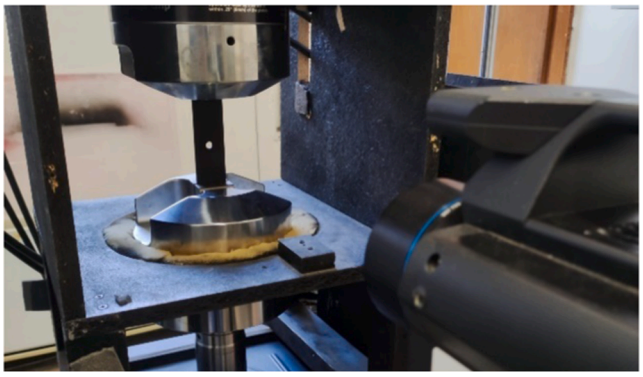

Fig. 2. Setup for fatigue tests, used for crack generation and TSA tests.

The influence of the current levels was investigated for titanium material, while, the tests on steel specimens were carried out considering the maximum current value (100 A), as resumed in Table 3.

It is also worth specifying that these are small fatigue cracks, real and closed, generated with a loading machine, and whose length was monitored and controlled with TSA analysis, post-processing the thermal signal acquired with a cooled sensor, an operation necessary to notice the presence of these cracks, stopping the fatigue tests, and return the machine to zero, after reaching a length of a few pixels.

2.3. *Preliminary results and proposed procedure for data analysis*

Considering the material properties here specified (from literature [14]) and fixed the specimen geometry (S1, Table 1), the phenomenon during the heating phase is simulated in case of titanium and two steels, and then also validated with experimental data in case of titanium alloy. The expected temperature increase for each material is reported in Table 4.

Fig. 4 reports the temperature trend in the case of titanium material, considering simulated and experimental data, and in particular a 3x3 regions of interest in different positions (area indicated in Fig. 4c), one in correspondence of the sound region (blue, ROI 1), another one in proximity of the crack tip (red, ROI 2), and the last one near the notch (green, ROI 3), together with two thermal maps after 0.1 s of heating and at the end of excitation. The temperature increases rate changes from the sound area to the crack tip since the observed areas experience different values of the density current. Fig. 1d reports the current distribution after the first instants of excitation, and as expected, the area around the crack tip presents the higher values of the density current. These qualitative results demonstrate that a significant and measurable temperature variation occurs in correspondence with the crack tip and then, a significant thermal contrast can be measured, already after the first instants of excitation. Of course, keeping the same geometry and considering the same time window, the temperature increase depends on the electrical and thermophysical properties of the material. As shown in

Fig. 3. Setup adopted for conduction thermography (a) together with its schematic representation (b), considering as main devices: (A) uncooled infrared sensor, (B) cooled infrared sensor, (C) specimen, (D) switching power supply, (E) resistors in parallel.

Table 3
Camera and excitation parameters for conduction tests; (the obtained current values are directly measured during the experiments and are referring to an effective value as average of different experiments, considering the resistors placed in parallel to the circuit, the cables and the thermal resistance of the specimen itself).

(a) Camera parameters					
Cooled camera FLIR X6540sc, lens 50 mm, MWIR 3–5 μm, temperature range 12.7 – 86.4 °C, integration time 0.57 ms, NETD < 25 mK, windowing 320 x 204 pixels	Frame rate(Hz) 500	Resolution (mm/pixel) 0.15	Microbolometer camera FLIR A655sc, lens 25 mm, LWIR 7–14 μm, temperature range −40 – 150 °C, NETD < 30 mK, windowing 640 x 240 pixels	Frame rate (Hz) 100	Resolution (mm/pixel) 0.15

(b) Excitation Parameters – Switching power supply DC (83.3 A, 12 V)				
Specimen (ID)	Current (A)	Resistence (Ω)	Pulse duration (s)	Acquisition Time (s)
S1 Ti-6Al-4V	24 37 54 74	0.5 0.1 + 0.2 → 0.3 0.2 0.2 // 0.5 → 0.14	2	10
S1, S2, S3, S4, S5 Ti-6Al-4V, AISI 304, Fe360	100	0.1		

Table 4
Material properties used to evaluate the temperature increase.

Material	Electrical resistivity (Ω · m)	Density (kg/m^3)	Specific heat capacity (J/kg · K)	k Thermal conductivity (W/mK)	ΔT_{max} expected at the crack tip (°C)
titanium alloy Ti-6Al-4V	1.8E-06	4500	520	6.7	2.0
austenitic steel AISI 304	1.4E-06	8000	500	16.0	0.9
ferromagnetic steel Fe360	5.4E-07	8400	410	40.0	0.4

Table 4, the temperature variation at the crack tip is expected to be on half of the titanium one, and then with the imposed conditions (100 A and 1750 ms), it can become hard to detect cracks. In this regard, the FE model can be a useful tool to set the test parameters (current and excitation time) in order to the desired target temperature. The good agreement between experiments and simulations suggests that the crack interface likely involves partial contact or imperfect contact, where there are regions of direct contact interspersed with reduced contact areas. Cracks may not fully close at the tip due to various factors influencing the contact condition, but the reference in this case regards a microscopic scenario. The chosen thermal conductance value selected for the simulations reflects the realistic thermal behaviour resulting from this contact condition that can be changed on a microscopic scale based on the area selected for validation.

The raw thermal data were then analysed. In particular, most of the information derived from this technique is related to the analysis of the transient regime in the first instants of the heating, when the diffusion phenomena and the heat generated at the edges of the specimens where the potential difference is applied do not significantly influence the results.

To describe the procedure for crack tip evaluation and length estimation by CT, some results obtained for the titanium material (specimen S1) are reported, considering the best conditions available for the tests: maximum current level (100 A), surface covered by black coating and analysis of data acquired with the cooled sensor.

In Fig. 5 is possible to observe the trend of the thermal signal during the heating by considering a pixel taken in correspondence with the crack tip (square ROI – red outline) and a pixel in correspondence with the relative sound area (circular ROI – blue outline). The same graph also reports the trend in correspondence of the notch (green outline), with a significant temperature increase, and some thermographic raw maps during the thermal excitation (after 0.1 s, and at the end of the heating). The experimental data confirms a significant temperature increase both in correspondence of the crack tip and notch regions while sound regions experience a lower temperature variation.

The temperature trends reported in Fig. 5 are related to a signal belonging to a single pixel and then affected by noise. This serves to appropriately justify the choice to analyze the data with a specific algorithm, focusing on the first part of the heating, where the noise still covers the material response in the sound area, with a slope of about 0 and a very low expected R^2.

In fact, if the analysis is limited to a short time interval (i.e. a small number of frames), it is possible to notice a significant heating only at the crack tip. It can be noticed in Fig. 5 that, considering the signal related to a single pixel in the sound area, the level of the noise at the beginning of the heating is such that the effect of the heat source is still

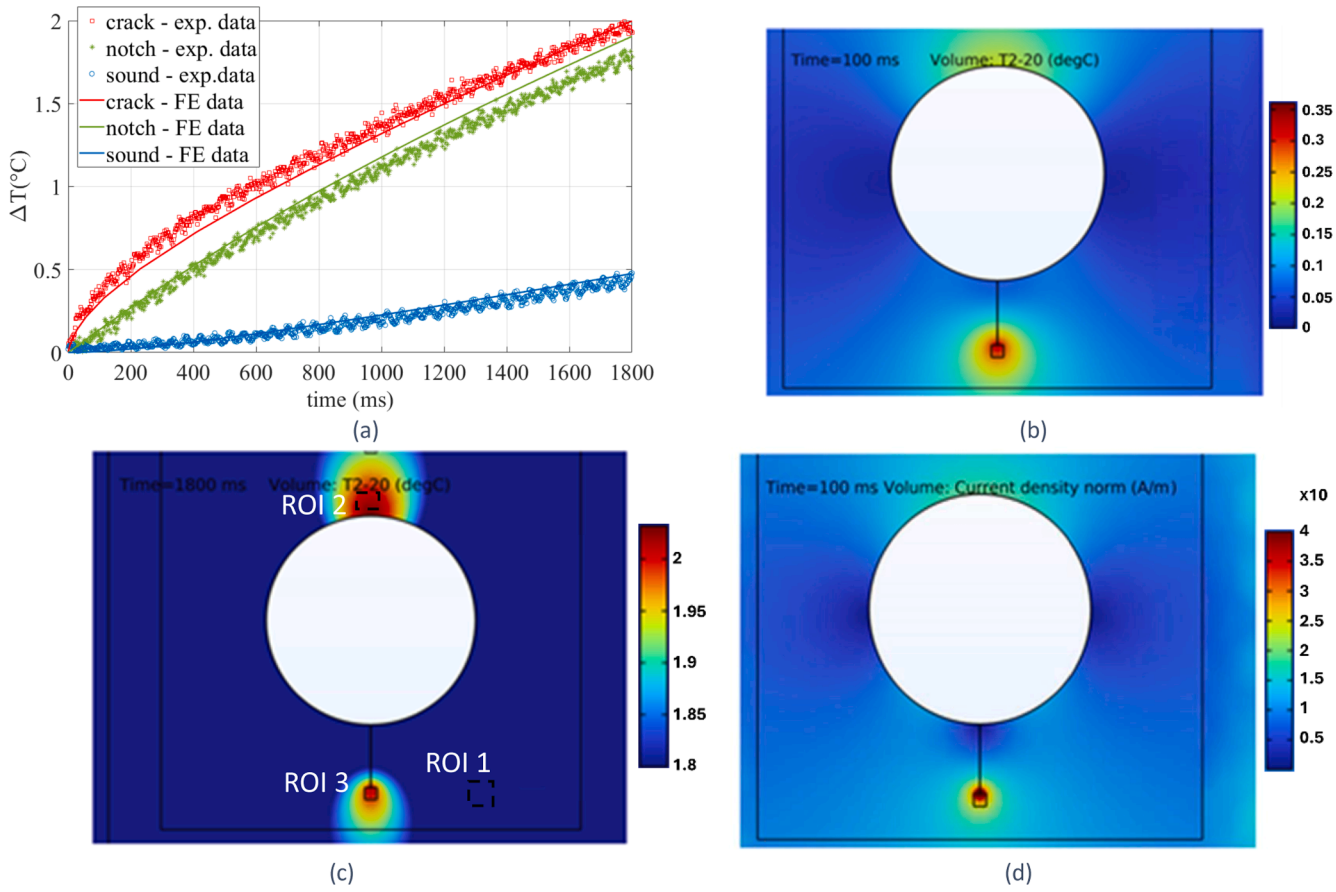

Fig. 4. COMSOL results: temperature increase in correspondence of a region with a crack, an area around the notch and the related sound area (a) with some thermal maps that represent the delta temperature after 0.1 s of excitation (b) and at the end of the same (c), and for completeness the map related to the current density distribution (d).

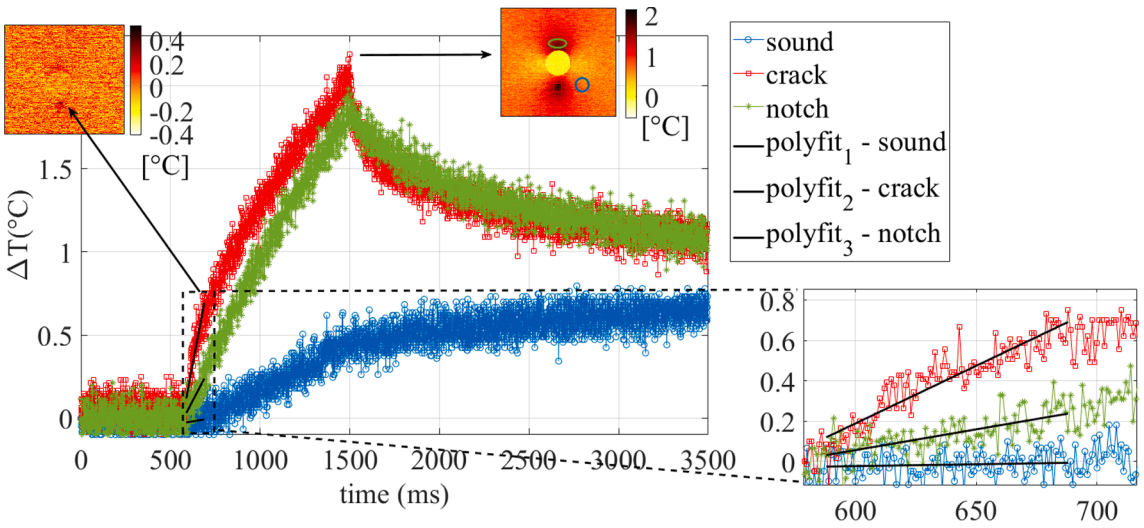

Fig. 5. Specimen S1, thermal behaviour after a conduction test, considering the reference sound area, a crack and the notch, with some thermal maps after 0.1 s of excitation and at the end of the long pulse heating (a zoom at the first instants of the heating).

negligible. Considering a time window of about 300 ms at the beginning of the heating phase, the temperature trend can be approximated as linear both for the sound and the crack regions. This means that the determination coefficient R^2 can be considered as an index for discerning the thermal behavior between the sound and the crack areas. Another index that can be used is the maximum signal reached by each pixel during the heating phase [23]. In this work, the procedure based on R^2 will be shown in detail since less affected by noise and has the advantage of requiring a very short heating phase.

Specifically, the R^2 pixel by pixel is calculated, expanding the analysis window one frame at a time [29,30], using a mobile truncation window size. All intervals start from the beginning of the heating. In

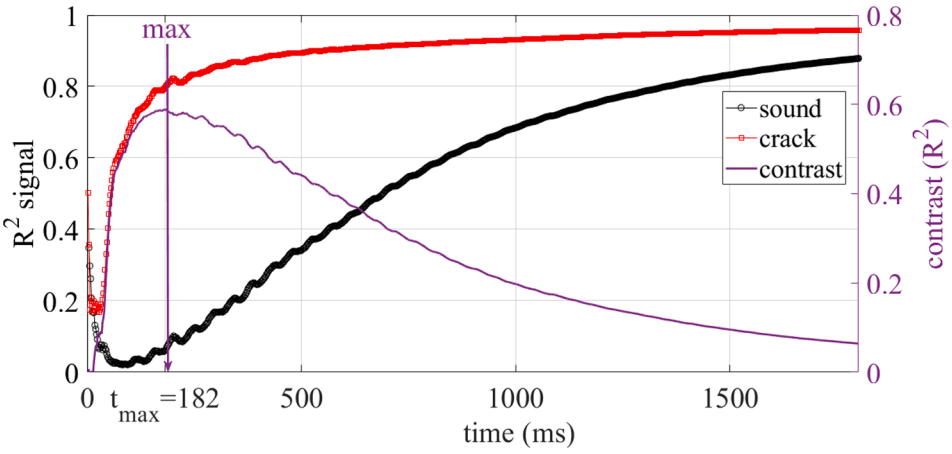

Fig. 6. Specimen S1, post processing of raw thermal data with R^2 after a conduction test, considering the signal at reference sound area and the signal at crack tip, reporting on the y-axis right the contrast in terms of R^2.

Fig. 6 is shown the trend of R^2 over time considering the average value of 3x3 ROIs in the sound and crack tip area, respectively. The R^2 contrast (purple line) changes over time an reaches its maximum value for a specific time interval.

Considering the R^2 signal in correspondence of a sound ROI as reported in Fig. 6 (black line) is possible to obtain also a sequence related to the R^2 contrast, subtracting this reference value pixel by pixel at the previous result.

Examining the R^2 map obtained in correspondence of the maximum contrast and considering a profile along the direction of crack growth, it is possible to observe a typical trend characterized by a noisy signal that oscillates around low values of R^2, and then changes sign and increases at the crack tip (Fig. 7). To find the crack tip a threshold value was set equal to the mean value on the sound area plus two times the sound standard deviation. In this way, the crack tip position can be defined as the first pixel along the profile for which the R^2 contrast is beyond the imposed threshold value. Then, it is possible to estimate the crack length by knowing the mm/pixel. In order to evaluate the precision of the measurement, five consecutive horizontal profiles were analysed, and the result was averaged to obtain the information related to the crack tip and relative lengths. For completeness, the Fig. 7 also reports the areas chosen to identify the sound area and to determine the threshold value and the absolute contrast in correspondence with the crack tip (red outline).

To evaluate the crack length, it is necessary to uniquely identify the notch edge. In this work, the Sobel edge algorithm has been applied to the sequence of raw thermal data, to extract the coordinates in correspondence of the notch geometries and have the same reference valid for all the tests and measurements (Fig. 8).

The thermoelastic data were analysed according to the procedure proposed in [10]. In particular, the procedure involves the signal reconstruction algorithm based on least squares method of thermal signal via IRTA 2 software (DES – Diagnostic Engineering Solutions) to assess the phase and amplitude of the first harmonic as features [11,31]. The procedure is applied to each pixel of the thermal data sequence and then first harmonic phase and amplitude maps are provided. The amplitude and phase are jointly used to find the crack tip position and finally a profile along the crack propagation direction is plotted.

To the purpose of evaluating the crack length, in present research, an average profile along the direction of crack propagation in the phase map was considered after the evaluation of 5 consecutive profiles, as in the case of CT analysis.

It is worth to mention that:

- the CT data refer to the sequences acquired with the cooled sensor and the specimens covered with black coating to be consistent with TSA analyses
- the analysis of TSA data is limited to phase map as it is the one of the consolidated procedure to evaluate crack tip [31–35].

To summarize the proposed procedure for data analysis in case of CT, below a bulleted list of the fundamental steps is reported:

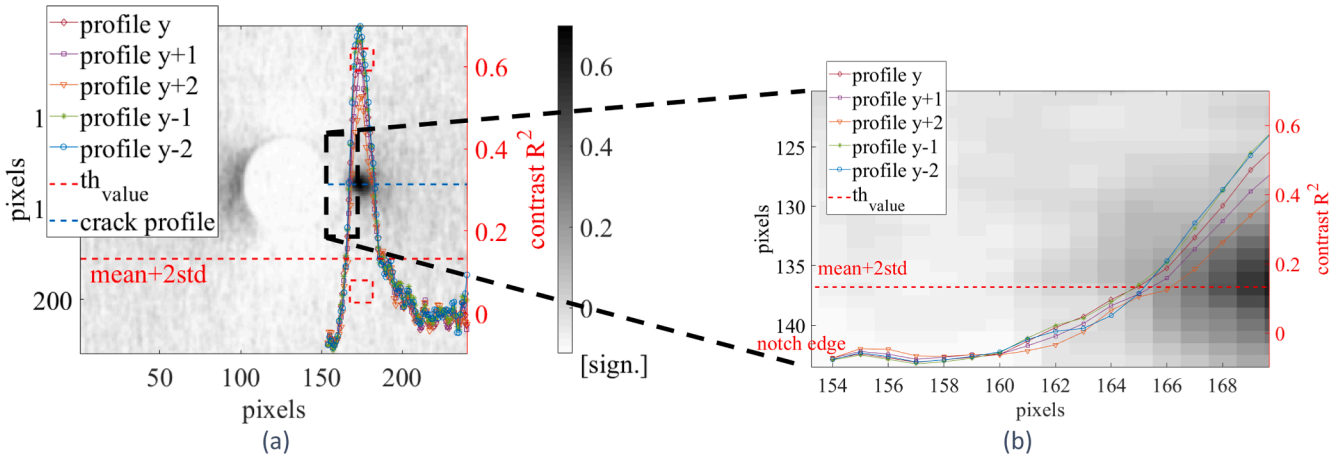

Fig. 7. Evaluation of the crack tip with conduction thermography – map of R^2 expressed in terms of contrast (after 0.16 s of excitation) and profiles for identification (a), with a zoom in the area of interest (b).

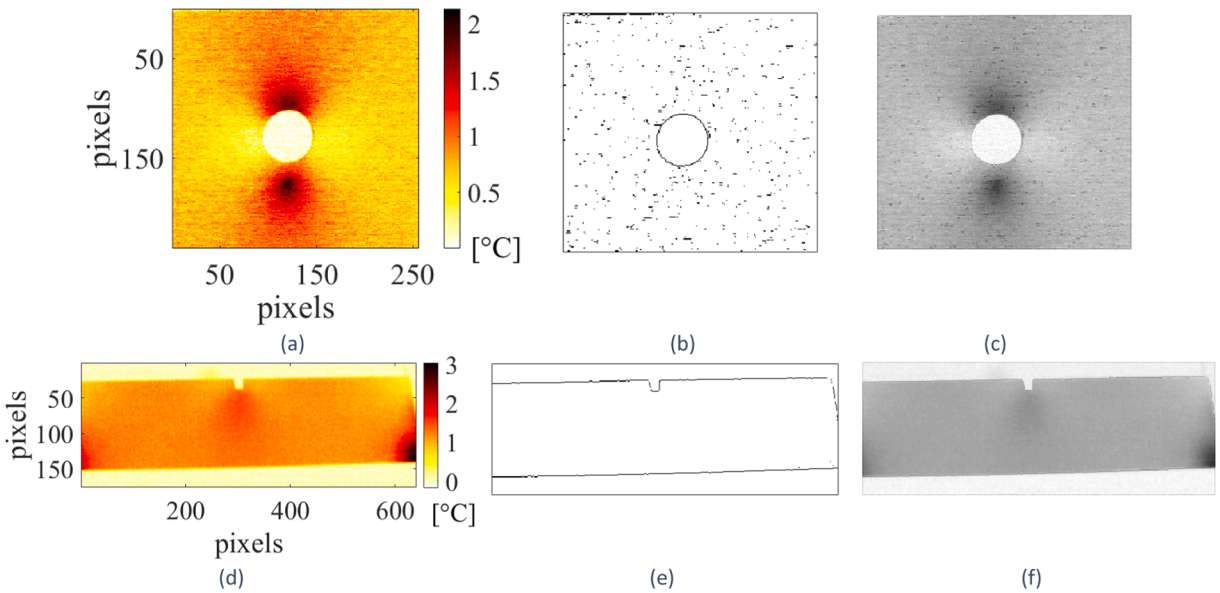

Fig. 8. Specimen S1. Edge detection – application of Sobel operator to identify the edges of the notch: case 1 – hole – (a) generic map of raw thermal data, (b) edge detection, (c) image overlay to identify directly the contour on the thermal result; case 2 – square notch – (d) generic map of raw thermal data, (e) edge detection, (f) image overlay to identify directly the contour on the thermal result.

- Analysing the heating phase with a linear approximation of the data pixel per pixel, changing the truncation window size one frame per time;
- Saving the R^2 map for each time interval to obtain a sequence of processed data related to the R^2 signal (the number of frames available coincides with the number of time intervals analysed);
- Extracting the R^2 signal in correspondence of a sound region (mean and standard deviation);
- Obtaining the sequence related to the R^2 contrast, subtracting pixel by pixel the mean value of the sound region;
- Analysing the R^2 contrast map in correspondence of the maximum value, calculated referring to the crack tip;
- Extracting notch edges with a Sobel filter (the operation has been done on the raw data, towards the end of the heating where the signal is quite clean from noise sources);
- Taking five different profiles along the crack growth direction, considering the average profile, and evaluating the crack length as number of pixels that do not exceed the threshold value, set as the mean of the sound plus two times the related standard deviation (the mm/pixel have to be known).

3. Results

This section shows a panoramic view of the obtained results considering different materials, whether different phenomena like heating current values, time of excitation, presence of a coating overlay, and material properties influence the mechanism of detection for CT. As already said, the electrical resistance of the material plays a crucial role in heat generation, as well as the thermos-physical properties thermal conductivity, specific heat, and diffusivity. Other practical considerations such as the presence or absence of a thin layer of black coating will be discussed showing the experimental results in the two different cases. In this application, and for the purpose of crack detection as surface defects, this black coating acts as an insulator to increase mainly the emissivity especially in case of steel material inspection, resulting, basically, in a higher thermal contrast.

The influence of these testing parameters will be discussed in detail presenting the experimental obtained results for the analysis of the titanium. For the specimen indicated as S1, in fact, the investigation mainly regards the influence of the IR sensors, emissivity surface and current value.

A first comparison between the two techniques is shown in Fig. 9, considering the TSA data in terms of contrast phase map, Fig. 9a, and the result obtained in the case of CT application, Fig. 9a, using the same sensor, covered the surface with black coating as in case of TSA, and reaching the highest available current level of 100 A, adopting the procedure previously explain to obtain the R^2 contrast map. The results in both cases reveal the presence of a crack on the right side.

In Fig. 10, the maps related to the same specimen S1 of Fig. 9 obtained with CT technique by using the uncooled sensor and with and without black coating are reported. Moreover, the trend of the R^2 signal along the crack growth direction (blue profile) is represented in the same maps. Another black dotted line represents the threshold value chosen to determine the crack tip position. In terms of absolute contrast, the result in Fig. 10a, using an uncooled sensor, is similar to the previous result obtained in the same test on the opposite side, but with a cooled sensor (Fig. 9b). However, as expected, the results are affected by a high level of noise if compared to the ones obtained with the cooled sensor (Fig. 7), with an absolute contrast that decreases along the crack tip, but still exceeds the threshold value chosen for defect identification by several pixels ($averageemissivityvalue\varepsilon_m = 0.65$[36]).

The influence of the current level is then analysed in detail for the "worst" case, reporting the results obtained in Fig. 11, where further decreasing the current value is further reduced to determine the limits of the technique for a fixed specimen geometry. The results show that, up to a current level of 54 A the crack can still be identified.

The frame at the maximum R^2 contrast occurs consistently at the same time: for the cooled sensor, it is about 100 frames (0.2 s of excitation), instead, for the uncooled sensor, the frames are about 30 (0.3 s of excitation). In the case of a current level of 54 A, the time of excitation corresponding to the maximum contrast increases slightly because it is necessary to wait a longer time to have a sufficient signal at the crack tip. Diffusion phenomena increase as the heating time increase and can affect the determination of the crack tip, as shown in Fig. 11 b.

Fig. 12 graphically reports the trend related to the normalised contrast for the uncooled sensor, changing the current value as testing parameters and analysing the data with the R^2 algorithm. The results demonstrate, as a current of 54 A is still enough to detect crack without black coating. The current level could decrease furtherly for high emissivity values, maintaining detection capability.

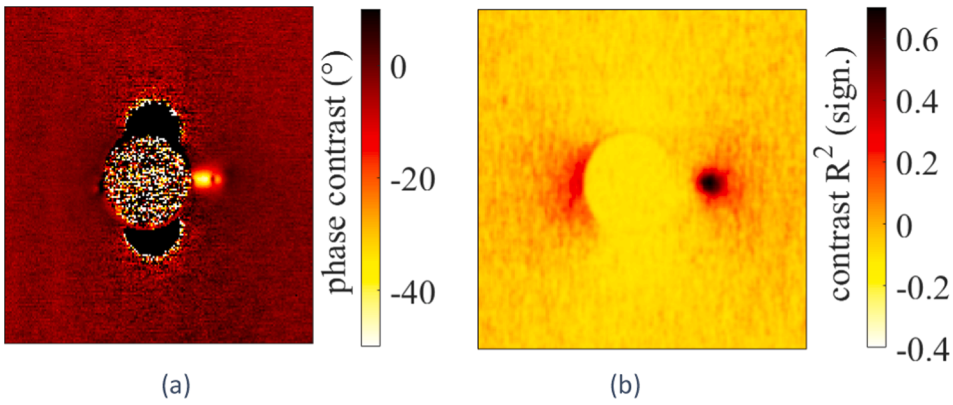

Fig. 9. Specimen S1. TSA, contrast phase map (a) vs CT result, R^2 contrast map – cooled sensor, 100 A, coated surface (b).

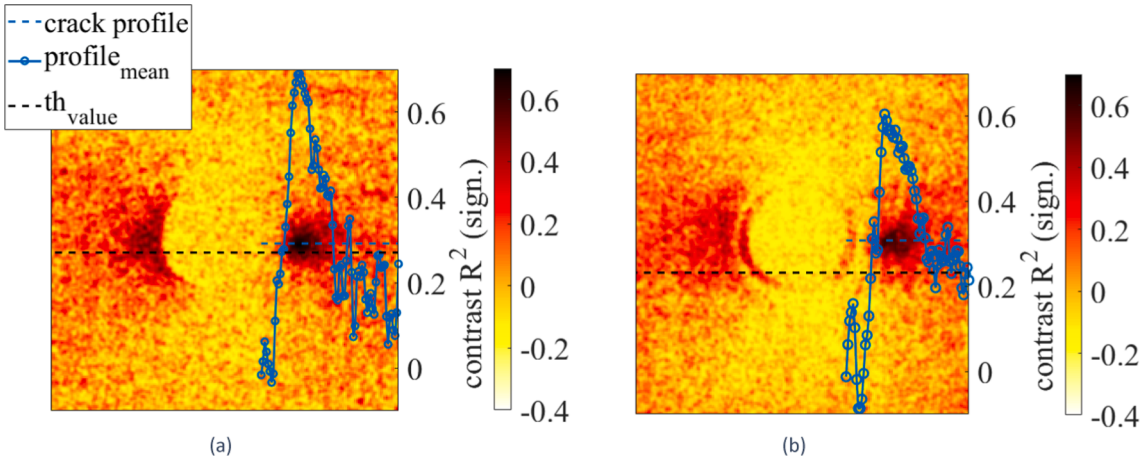

Fig. 10. Specimen S1. CT results R^2 contrast maps in case of uncooled sensor, 100 A – coated surface (a) and uncoated surface (b).

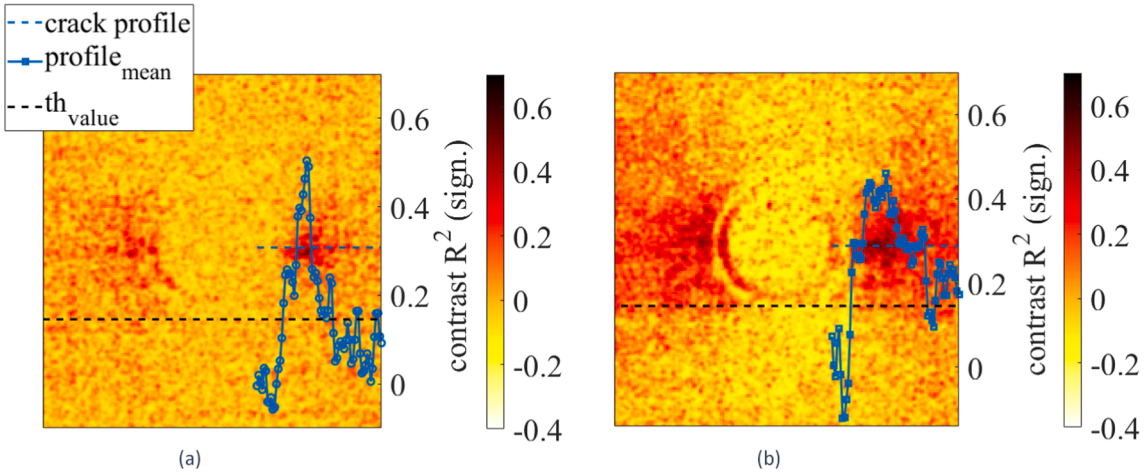

Fig. 11. Specimen S1. CT results, R^2 contrast maps, uncooled sensor and uncoated surface, evaluation of the current value – 74 A (a) vs 54 A (b).

Figs. 13 and 14 show a comparison between the TSA and CT, for a current of 100 A, using a cooled sensor and a black coating. The cracks produced in these cases are very small, as shown by the TSA results. The phase signal inversion occurs very close to the notch region.

Except for the smallest crack for the specimen indicated as S2, the TSA results show a phase contrast that is very similar for all cracks, regardless of the crack length and material. The CT results reveal an absolute contrast in correspondence of the crack tip, as the previous cases, always higher than the threshold value. As in the case of the TSA results, the choice of the correct pixel identifying the notched edge is fundamental and has a strong influence on the correct measurement of the crack length. Referring to the specimens with two cracks (S2 and S3), the map chosen to represent the CT results is the one that provides the length for the longest crack; however, the difference in terms of maximum contrast for the two cracks is only of 2–3 frames.

For both techniques, the areas selected to obtain the reference or

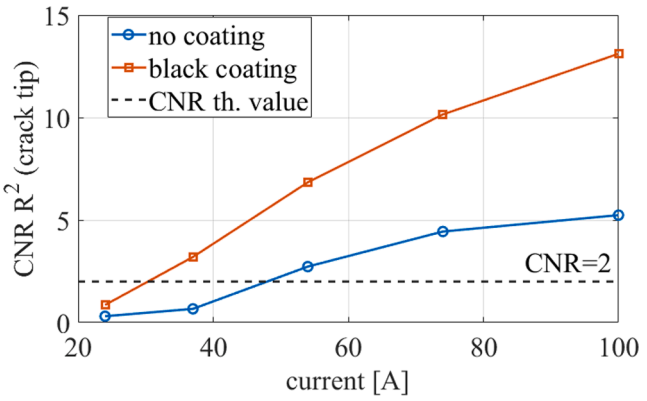

Fig. 12. Specimen S1. CT results, evaluation of the normalized contrast in terms of R^2 at the crack tip when the current changes, uncooled sensor coated and uncoated surface.

sound signal for the two cracks are different, but they are chosen to represent a single result and a single map, as they were similar in the two cases.

4. Discussion

Table 5 reports the quantitative results in terms of crack length estimation in the case of the analysis of titanium material, considering the maps reported before in Figs. 9, 10, 11 and 12, for TSA and CT. In the case of TSA, the error of the measurement was estimated considering the measure of a pixel, and so the obtained geometrical resolution. For CT, the error of the measurement is the standard deviation of three consecutive measurements, repeated as separate tests on the same specimen. Where this value is lower than the measure of a pixel, the value of the geometrical resolution, was reported. The results in terms of the absolute measure of the crack length are identical in all the cases reported in Table 5. Only in the case of specimen without coating, the values are higher due to the noise of the test itself. In fact, in case of inspection without coating, the emissivity variation influences, obviously, the obtained results. Furthermore, it is necessary to underline again that this estimation regards short fatigue cracks, containing few pixels (in this case 13 pixels, with a difference of just 3–4 pixels among tests). However, the values obtained for the three different currents are not statistically inconsistent with each other. In this regard, Table 5 reports also the values with the confidence interval at the 95 % level, together with the indication of the p_{value} ($p_{value} \geq 0.05 - significancelevel$) obtained after an ANOVA analysis to demonstrate that there is no significant difference in the crack length estimation as the current changes.

Table 6 summarizes the results obtained by analysing steels S2, S4, S3 (Figs. 13 and 14). Also, in this case, the estimation of the absolute crack length is referred to both techniques TSA and CT. As explained before, the value of the standard deviation is also evaluated, as for the previous cases. For CT, the standard deviation related to the three tests, always returned lower results compared to the value of the geometric resolution, and so, for this reason, the error corresponds to the geometrical resolution itself. The results in terms of crack length are always comparable and differ at most by the value of one pixel. In this case, the definition of short fatigue cracks is even more fitting than the previous case because the results refereed to cracks no larger than 1 mm.

5. Conclusions

This work has proven the feasibility of conduction thermography in short fatigue crack detection and quantitative characterization, investigating different materials and analysing some thin specimens. Considering the adopted set-up, with low-cost devices, in terms of energy source and sensor, with low current values, it has been demonstrated the possibility to obtain quantitative results, in terms of crack length estimation, in agreement with those achieved via the TSA technique, furthermore with some advantages as the capability to inspect surface without black coating and offline. The results demonstrate that the success of CT technique depends on the material's electrical properties and the electrical current required to have a sufficient signal in correspondence with the crack tip.

For the first time in literature, the quantitative results referred to a titanium alloy, which represents a perfect candidate for the potential application of the technique, with concrete and industrial possibility concerning the type of investigated defects and analysed geometries.

Some testing parameters, such as current level and type of IR sensor, have been investigated in detail, and the results demonstrated the

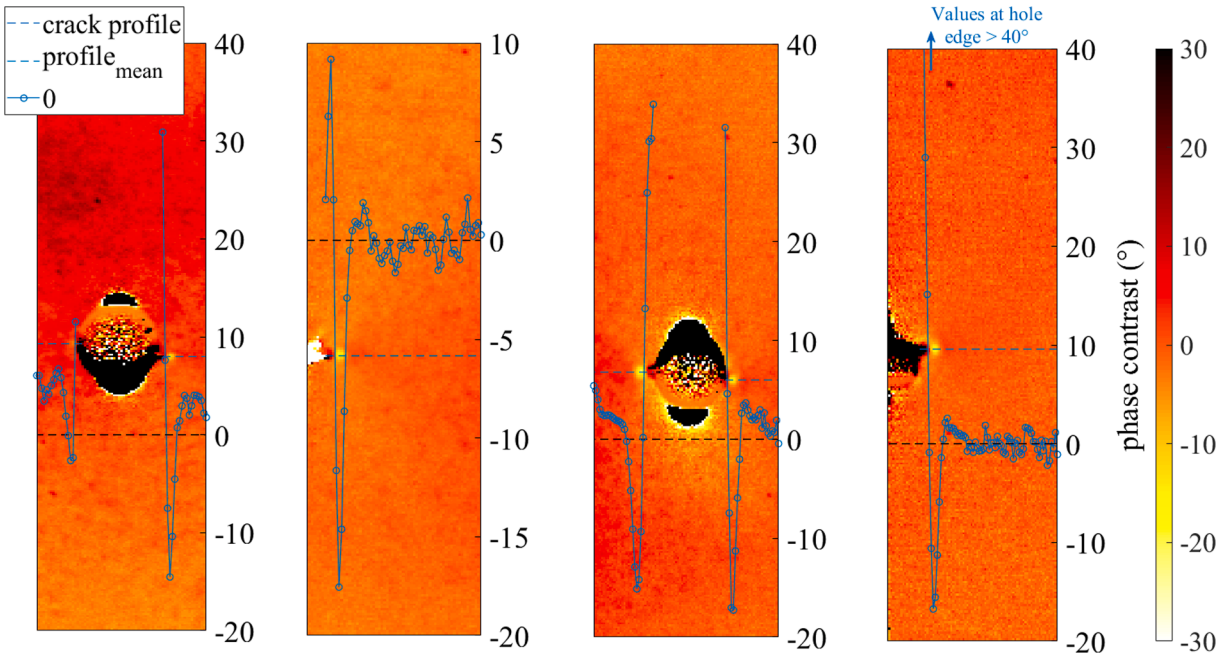

Fig. 13. TSA results, contrast phase maps, specimen S2 AISI 304 (a), specimen S4 AISI 304 (b), specimen S3 Fe360 (c), specimen S5 Fe360.

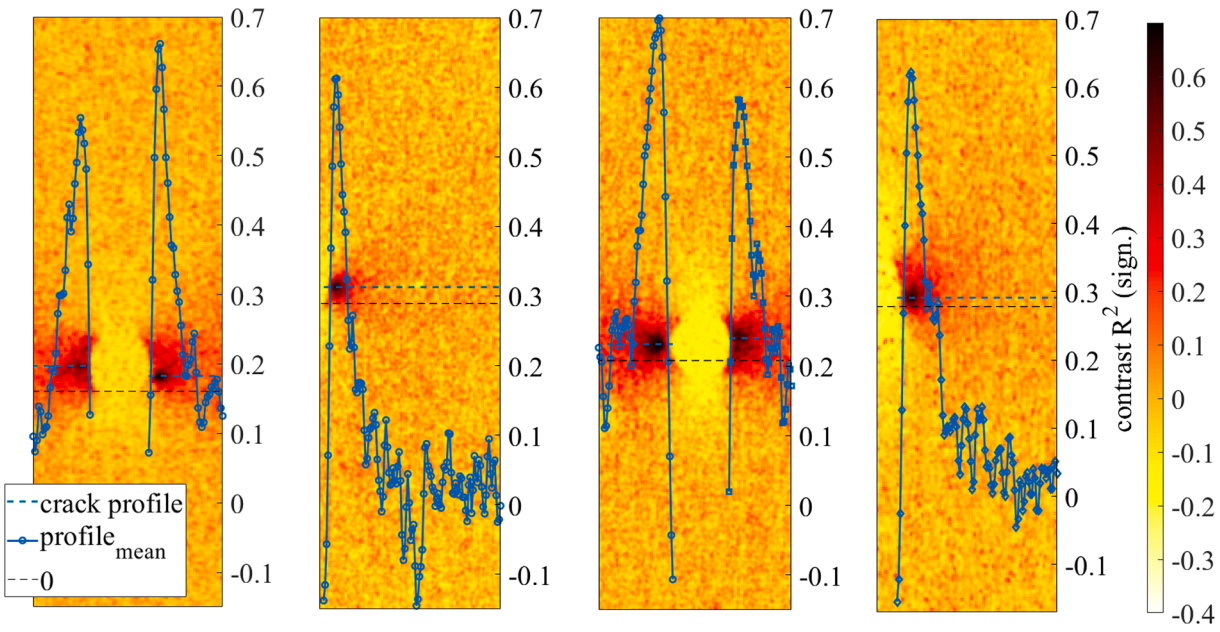

Fig. 14. CT results, R^2 contrast maps, cooled sensor, 100 A, coated surfaces, specimen S2 AISI 304 (a), specimen S4 AISI 304 (b), specimen S3 Fe360 (c), specimen S5 Fe360.

Table 5
Specimen S1, crack length estimation comparing TSA and CT results related to the previous Figs. 9, 10, 11 and 12.

	TSA	CT	CT	CT		
Type of sensor	**cooled**	**cooled**	**uncooled**	**uncooled**		
Surface	**coated**	**coated**	**coated**	**uncoated**		
Current level (A)	/	**100**	**100**	**100**	**74**	**54**
S1 – Titanium Crack length (mm) mean value ± standard deviation	1.95 ± 0.15	1.95 ± 0.15	1.95 ± 0.15	2.10 ± 0.18	2.40 ± 0.24	1.80 ± 0.24
S1 – Titanium Crack length (mm) mean value ± confidence interval 95 %				2.10 ± 0.37 ANOVA analysis – p_{value} = 0.0787	2.40 ± 0.74	1.80 ± 0.74

Table 6
Specimens S2, S3, S4 and S5, crack length estimation (mm) comparing TSA and CT results related to the previous Figs. 13 and 14. To be noticed the dimension of the pixel is 0.15 mm.

Specimen	TSA cooled coated sx	TSA cooled coated dx	CT cooled coated 100 A sx	CT cooled coated 100 A dx
S2 – AISI 304	0.15 ± 0.15	0.45 ± 0.15	0.30 ± 0.15	0.45 ± 0.15
S4 – AISI 304		0.75 ± 0.15		0.90 ± 0.15
S3 – Fe360	0.75 ± 0.15	0.45 ± 0.15	0.75 ± 0.15	0.45 ± 0.15
S5 – Fe360		1.15 ± 0.15		0.90 ± 0.15

possibility of recognizing short cracks, up to 0.3–0.5 mm.

The main novelty of this work regards the proposed procedure to analyse raw thermal data. More specifically, the proposed algorithm consists of considering the R^2 coefficient as an index to describe the first instants the thermal behaviour of the material during the heating phase.

Future developments will investigate the possibility of using the proposed technique and procedure for quantitative analysis in crack growth monitoring to demonstrate its possible application as a structural health monitoring (SHM) technique.

Finally, the simulated and experimental results shown the analogy between temperature variations due to thermoelastic effect and current distribution around different types of notches and cracks. The possible relationship between the two techniques and the potential analogy between current and stress distribution will be investigated in future works.

Funding

Part of the work has been Financed by the European Union - Next-GenerationEU (National Sustainable Mobility Center CN00000023, Italian Ministry of University and Research Decree n. 1033–17/06/2022, Spoke 11 - Innovative Materials & Lightweighting). The opinions expressed are those of the authors only and should not be considered as representative of the European Union or the European Commission's official position. Neither the European Union nor the European Commission can be held responsible for them.

Data availability statement

The data presented in this study are available on request from the corresponding author.

CRediT authorship contribution statement

Ester D'Accardi: Writing – review & editing, Writing – original draft, Validation, Investigation, Formal analysis, Data curation, Conceptualization. **Rosa De Finis:** Writing – review & editing, Writing – original draft, Software, Formal analysis, Data curation, Conceptualization. **Giuseppe Dell'Avvocato:** Writing – review & editing, Methodology, Data curation. **Giuseppe Masciopinto:** Writing – review & editing, Methodology, Data curation. **Davide Palumbo:** Writing – review & editing, Writing – original draft, Software, Investigation. **Umberto Galietti:** Writing – review & editing, Supervision, Resources, Project administration, Investigation, Funding acquisition, Conceptualization.

Declaration of competing interest

The authors declare that they have no known competing financial interests or personal relationships that could have appeared to influence the work reported in this paper.

References

[1] P.P. Milella, Fatigue and Corrosion in Metals, Springer Science & Business Media, 2012.
[2] Y. Kong, C.J. Bennett, C.J. Hyde, A review of non-destructive testing techniques for the in-situ investigation of fretting fatigue cracks, Mater. Des. 196 (2020) 109093.
[3] W.K. Wong, S.H. Ng, K. Xu, A Statistical investigation and optimization of an industrial radiography inspection process for aero-engine components, Qual. Reliab. Eng. Int. 22 (3) (2006) 321–334.
[4] A. Upadhyay, J. Li, S. King, S. Addepalli, A deep-learning-based approach for aircraft engine defect detection, Machines 11 (2) (2023) 192.
[5] DIN EN 17119, Non-destructive testing - Thermographic testing - Active thermography, 2018-10.
[6] B. Weekes, D.P. Almond, P. Cawley, T. Barden, Eddy-current induced thermography—probability of detection study of small fatigue cracks in steel, titanium and nickel-based superalloy, NDT E Int. 49 (2012) 47–56.
[7] V. Ageeva, T. Stratoudaki, M. Clark, M.G. Somekh, November). Integrative solution for in-situ ultrasonic inspection of aero-engine blades using endoscopic cheap optical transducers (CHOTs), in: Proceedings of the 5th International Symposium on NDT in Aerospace, 2013, pp. 13–15.
[8] S. Hirsekorn, P.W. Van Andel, U. Netzelmann, Ultrasonic methods to detect and evaluate damage in steel, Nondestruct. Testi. Eval. 15 (6) (1998) 373–393.
[9] J.M. Vasco-Olmo, M.N. James, C.J. Christoper, E.A. Patterson, Assessment of crack tip plastic zone size and shape and its influence on crack tip shielding, Fatigue Fract. Eng. Mater. Struct. 39 (2016) 969–981.
[10] G. Pitarresi, E.A. Patterson, A review of the general theory of thermoelastic stress analysis, J. Strain Anal. 40 Eng. Design 38 (5) (2003) 405–417.
[11] F. Ancona, D. Palumbo, R. De Finis, G.P. Demelio, U. Galietti, Automatic procedure for evaluating the Paris Law of martensitic and austenitic stainless steels by means of thermal methods, Eng. Fract. Mech. 163 (2016) 206–219.
[12] J. Vrana, M. Goldammer, K. Bailey, M. Rothenfusser, W. Arnold, Induction and conduction thermography: optimizing the electromagnetic excitation towards application, in: AIP Conference Proceedings (vol. 1096, No. 1), American Institute of Physics, 2009, pp. 518–525.
[13] P. Jäckel, U. Netzelmann, The influence of external magnetic fields on crack contrast in magnetic steel detected by induction thermography, Quant. Infr. Therm. J. 10 (2) (2013) 237–247.
[14] B. Oswald-Tranta, Detection and characterisation of short fatigue cracks by inductive thermography, Quant. Infr. Therm. J. 19 (4) (2022) 239–260.
[15] A. Salazar, A. Mendioroz, A. Oleaga, Flying spot thermography: quantitative assessment of thermal diffusivity and crack width, J. Appl. Phys. 127 (2020) 131101.
[16] R.A. Javier, M. Arantza, S. Agustin, Numerical modeling of static and flying spot thermography for narrow crack characterization. Proceedings of the 2021 International Conference on Quantitative InfraRed Thermography, Paris, Fance, 2022.
[17] J. Vrana, M. Goldammer, Defect detection mechanisms with induction and conduction thermography: current flow and defect-specific warming, Quant. Infr. Therm. J. 17 (2) (2020) 130–151.
[18] J. Vrana, M. Goldammer, U. Netzelmann, Induction and conduction thermography. A new surface inspection method suited for the forging industry. Proceedings of the 20th International Forgemasters Meeting, Graz, Austria, 2017.
[19] T. Sakagami, K. Ogura, S. Kubo, Development of thermographic NDT for the damage inspection in carbon fiber reinforced plastics, in: The First US-Japan Symposium on Advances in NDT, Oahu, Hawaii, 1996, pp. 420–425.
[20] T. Sakagami, K. Ogura, New flaw inspection technique based on infrared thermal images under Joule effect heating, JSME Int. J. A Mech. Mater. Eng. 37 (4) (1994) 380–388.
[21] B. Oswald-Tranta, Induction thermography for surface crack detection and depth determination, Appl. Sci. 8 (2) (2018) 257.
[22] B. Oswald-Tranta, A. Hackl, L. de Uralde, P. Olavera, E. Gorostegui-Colinas, A. Rosell, Calculating probability of detection of short surface cracks using inductive thermography, Quant. Infr. Therm. J. (2022) 1–20.
[23] E. D'Accardi, D. Palumbo, R. De Finis, U. Galietti, Detection and characterization of short fatigue cracks by conduction thermography, Eng. Proc. 51 (1) (2023) 23.
[24] L. Santoro, V. Razza, M. De Maddis, Frequency-based analysis of active laser thermography for spot weld quality assessment, Int. J. Adv. Manuf. Technol. 130 (5) (2024) 3017–3029.
[25] J. Rodríguez-Aseguinolaza, M. Colom, J. González, A. Mendioroz, A. Salazar, Quantifying the width and angle of inclined cracks using laser-spot lock-in thermography, NDT E Int. 122 (2021) 102494.
[26] J. Schlichting, M. Ziegler, A. Dey, C. Maierhofer, M. Kreutzbruck, Efficient data evaluation for thermographic crack detection, Quant. Infr. Therm. J. 8 (1) (2011) 119–123.
[27] G.D. Addante, G. Dell'Avvocato, F. Bisceglia, E. D'Accardi, D. Palumbo, U. Galietti, Laser thermography: an investigation of test parameters on detection and quantitative assessment in a finite crack, Eng. Proc. 51 (1) (2023) 7.
[28] P. Myrach, M. Ziegler, C. Maierhofer, M. Kreutzbruck, Influence of the acquisition parameters on the performance of laser-thermography for crack detection in metallic components, in: AIP Conference Proceedings (vol. 1581, No. 1), American Institute of Physics, 2014, pp. 1624–1630.
[29] E. D'Accardi, D. Palumbo, V. Errico, A. Fusco, A. Angelastro, U. Galietti, Analysing the probability of detection of shallow 44 spherical defects by means of pulsed thermography, J. Nondestrct. Eval. 42 (1) (2023) 27.
[30] G. Dell'Avvocato, D. Palumbo, Thermographic procedure for the assessment of Resistance Projection Welds (RPW): investigating parameters and mechanical performances, J. Adv. Join. Process. 9 (2024). ISSN 2666-3309.
[31] R. De Finis, D. Palumbo, F. Di Carolo, M. Ricotta, G. Meneghetti, U. Galietti, Crack tip position evaluation and Paris' law assessment of a propagating crack by means of temperature-based approaches, Procedia Struct. Integrity 39 (2022) 528–545.
[32] F.A. Diaz, E.A. Patterson, R.A. Tomlinson, R.A. Yates, Measuring stress intensity factors during fatigue crack growth using thermoelasticity, Fract. Eng. Mater. Struct. 27 (7) (2004) 571–1513.
[33] ASTM E 647–00, Standard test method for measurement of fatigue crack growth rates, 2004.
[34] G. Meneghetti, P. Lazzarin, Significance of the elastic peak stress evaluated by FE analyses at the point of singularity of sharp VNotched components, Fatigue Fract. Eng. Mater. Struct. 30 (2) (2007) 95–106.
[35] R.A. Tomlinson, E.A. Patterson, examination of crack tip plasticity using thermoelastic stress analysis, thermomechanics and infra-red imaging, in: Proceedings of the Society for Experimental Mechanics Series 2011, vol. 7, Springer, New York, NY, 2011.
[36] ASTM, A., 14: Standard Practice for Measuring and Compensating for Emissivity Using Infrared Imaging Radiometers, West Conshohocken, PA, 19428, 1933.